PERGAMON

Engineering Fracture Mechanics 64 (1999) 141–159

Engineering Fracture Mechanics

www.elsevier.com/locate/engfracmech

Effect of modelling of traction and thermal singularities on accuracy of SIFS computation through modified crack closure integral in BEM

N.K. Mukhopadhyay[a, 1], S.K. Maiti[b,*], A. Kakodkar[a, 1]

[a] *Reactor Design and Development Group, Bhabha Atomic Research Centre, Mumbai 400085, India*
[b] *Mechanical Engineering Department, Indian Institute of Technology, Bombay, Mumbai 400076, India*

Received 25 March 1999; received in revised form 8 June 1999; accepted 7 July 1999

Abstract

The effect of simultaneous modelling of both strain and traction singularities, and temperature derivative and heat flux singularities at the crack tip, on the accuracy of computation of stress intensity factors (SIFs) based on the modified crack closure integral in boundary element method is presented. Simple relations are given for SIF calculations. Results on mode I, mode II and mixed mode, crack subjected to mechanical and/or thermal loading are studied to illustrate the difference between partial and total modelling of the singularities. The dependence of accuracy of the SIFs on the crack tip element size is examined. The effect of order of Gaussian quadrature on the accuracy is also reported.

Keywords: Traction singularity; Heat flux singularity; Mechanical loading on crack; Thermal loading on crack; Modified crack closure integral; Stress intensity factor; Boundary element method; Gaussian quadrature; Accuracy of SIF computation

1. Introduction

Around an elastic crack tip there are both strain and stress singularities. When such a crack is analysed by the boundary element method (BEM), the stress singularity gives rise to the

* Corresponding author. Tel.: +91-22-576-7526; fax: +91-22-578-3480.
E-mail addresses: nirmalk@apsara.barc.ernet.in (N.K. Mukhopadhyay), skmaiti@me.iitb.ernet.in (S.K. Maiti)
[1] Tel.: +91-22-550-5050 Ext. 2586; fax: +91-22-550-5151.

0013-7944/99/$ - see front matter
PII: S0013-7944(99)00069-7

Nomenclature

a	crack length
c_n	coefficients of traction in MCCI formulation
E	elastic modulus
G_{I}, G_{II}	strain energy release rate in mode I, mode II
H_1, H_2	length
K_{I}, K_{II}	stress intensity factors
K_{T}	amplitude of thermal singularity
l	crack tip element size
L, W	geometric dimensions of domain
N_i	shape functions
p, q	components of crack edge loading normal and parallel to crack
r	distance from crack tip
r_1, r_2	internal and external radii
s_j, t_j	components of traction parallel and normal to crack
u, v	components of displacement parallel and normal to crack
W_{I}, W_{II}	crack closure work
x, y	Cartesian coordinates
Y	SIF correction factor
Y_1	Lewis form factor
θ	crack orientation with x-axis
ν	Poisson's ratio
ξ	natural coordinate
σ_{b}	Lewis's bending stress
α	coefficient of thermal expansion
ϕ	potential/temperature
λ	heat flux
ϑ	pressure angle

traction singularity on any artificial boundary passing through the crack tip. The analysis, therefore, calls for a simulation of both the singularities. In the heat conduction problems an analysis by the BEM also requires handling of singularities in both temperature derivative and heat flux. Though the difference between partial and total modelling of the singularities on the computation of SIFs has been brought out in the displacement method, the same is not yet clear when the calculations are done through the modified crack closure integral (MCCI) technique.

Barsoum [1] introduced a singularity element, commonly known as quarter point element, to simulate both strain and traction singularities at the crack tip in the finite element method (FEM). In the BEM, the displacement and traction are treated as two independent entities. The same quarter point element when employed in the BEM, ensures the strain singularity but not the traction singularity. Because of this the quarter point element is sometimes termed as 'strain singularity element' in the BEM.

The issue of simulating both the strain and traction singularities have received a considerable attention in the BEM [1–15]. Cruse and Wilson [2], Tan and Fenner [3], Nadiri et al. [6], etc., used only the strain singularity element and presented the improvement in the accuracy of the SIFs over the nonsingular elements. Blandford et al. [5] introduced a special crack tip element which ensured both the strain and traction singularities. In this element, termed as 'traction singularity element', the mid node is shifted to the quarter point to ensure the strain singularity and modified shape functions are introduced to account for the traction singularity. Mixed mode fracture analysis using the singularity boundary element is discussed by Van der Weeen [7]. Watson [15] employed the Hermitian cubic shape functions to characterise the singularity for straight and curved cracks under a plane strain condition. Aliabadi et al. [9,12] proposed a strategy, whereby an analysis is possible by removing the stress singularity at the crack tip.

In a heat conduction problem too there are singularities at the crack tip [16–17]. For example, Emery et al. [16] has pointed out that when the flow of heat is interrupted by a free boundary, e.g. crack edge, the field shows a singularity near the crack tip. When the analysis is performed using the FEM, the temperature derivative ($\partial\phi/\partial r$) singularity is only to be ensured. This may be achieved by employing the quarter point elements around the crack tip and one need not really bother separately about the singularity in the normal derivative/heat flux ($\partial\phi/\partial n$). However when the BEM is employed, singularities in both the radial derivative ($\partial\phi/\partial r$) and normal derivative ($\partial\phi/\partial n$) are to be accounted for a total modelling of the singularity. In the BEM, use of quarter point element can ensure a partial modelling, i.e. singularity in the temperature derivative is taken care of. The effect of simulating both the temperature derivative and heat flux singularities on the computation of SIFs using the BEM has been discussed by Katsareas and Anifantis [18] and Prasad et al. [19]. While Katsareas and Anifantis [18] have employed the quarter point element along with multiregion technique, Prasad et al. [19] have adapted the discontinuous quarter point element and the dual boundary element method (DBEM). In the case of thermal load problems there is a possibility of cumulative effect of partial or total modelling, since the heat conduction and stress analyses are to be done in stages.

In the BEM, displacement method is the most widely employed to evaluate the SIFs. J-integral has also been shown to be useful for the purpose [19]. Recently, an improvement in the accuracy of the SIFs through the MCCI technique over the displacement method has been reported [20–24]. The present authors [22–24] have demonstrated the effectiveness of this method for both mechanical and thermal loading. In these calculations only the derivative singularities have been considered.

In this paper, the effect of partial and total modelling of the singularities at the crack tip on the computation of SIFs through the MCCI method is presented in the case of mechanical and/or thermal loading. Examples of mode I, mode II or mixed mode are considered.

In the BE analysis employing the conventional elements, while evaluating the coefficients of the simultaneous equations the singularity term involved is just a logarithmic singularity, i.e. $\ln(1/r)$. Usually, a four point Gaussian quadrature is considered alright for the numerical integration. This situation changes, when the singularity elements are employed. Specially there is a product of two singularity terms when the crack tip is surrounded by traction/heat flux singularity elements. How does the order of Gauss quadrature affect the accuracy of the SIFs is an open question. It is a common experience that the accuracy of the SIFs is dependent on

the crack tip element size in the displacement method. How does the size of the traction/heat flux singularity element influence the accuracy of the MCCI based calculation of the SIFs is also not yet examined. These issues are also addressed in this paper.

2. Computation of stress intensity factors

In the traction singularity element [6,8] displacement has a $\sqrt{r}$ variation near the crack tip (Fig. 1). It can be represented by

$$v = N_1\ v_{j-2} + N_2\ v_{j-1} + N_3 v_j, \tag{1}$$

where $N_1 = \xi(\xi-1)/2$, $N_2 = (1-\xi^2)$ and $N_3 = \xi(\xi+1)/2$ are the usual shape functions. It is straightforward to show

$$v = (2\ v_{j-2} - 4v_{j-1})(1 - x/l) + (4v_{j-1} - v_{j-2})\sqrt{(1 - x/l)}, \tag{2}$$

where l is the crack tip element length and $\sqrt{(r/l)} = (1 - \xi)/2$. The traction t can be similarly expressed as follows [5]

$$t = N_1 t_1 + N_2\ t_2 + N_3 t_3 = \underline{\boldsymbol{N}}_1\ \underline{\boldsymbol{t}}_1 + \underline{\boldsymbol{N}}_2 \underline{\boldsymbol{t}}_2 + \underline{\boldsymbol{N}}_3 \underline{\boldsymbol{t}}_{3,}, \tag{3}$$

where $\underline{\boldsymbol{N}}_1 = N_1\sqrt{(l/r)}$, $\underline{\boldsymbol{N}}_2 = N_2\sqrt{(l/r)}$, $\underline{\boldsymbol{N}}_3 = N_3\sqrt{(l/r)}$, and

$$\underline{\boldsymbol{t}}_1 = \lim_{r\to 0}\ t_1\ \sqrt{(r/l)} = t_j,$$

$$\underline{\boldsymbol{t}}_2 = t_2/2 = t_{j+1},$$

$$\underline{\boldsymbol{t}}_3 = t_3 = t_{j+2}.$$

Finally t can be expressed as follows:

$$t = t_j\sqrt{(l/r)} + (-t_{j+2} + 4\ t_{j+1} - 3t_j) + (2t_{j+2} - 4\ t_{j+1} + 2t_j)\sqrt{(r/l)}. \tag{4}$$

It is relevant to note here that t_j and t_{j+1} are not the nodal tractions, they are rather traction multiplied by $\sqrt{(r/l)}$. The relations presented in the following for calculation of the SIFs are, however, expressed in terms of amended tractions t_j, t_{j+1} and t_{j+2}, which are directly available from a standard boundary element analysis using the traction singularity element.

2.1. Remote mechanical loading

When a component is subjected to mechanical loading away from the crack edge (Fig. 1a), the mode I crack closure work is given by the following [22]

$$W_{\mathrm{I}} = \tfrac{1}{2}\int_0^l vt\ \mathrm{d}x, \tag{5}$$

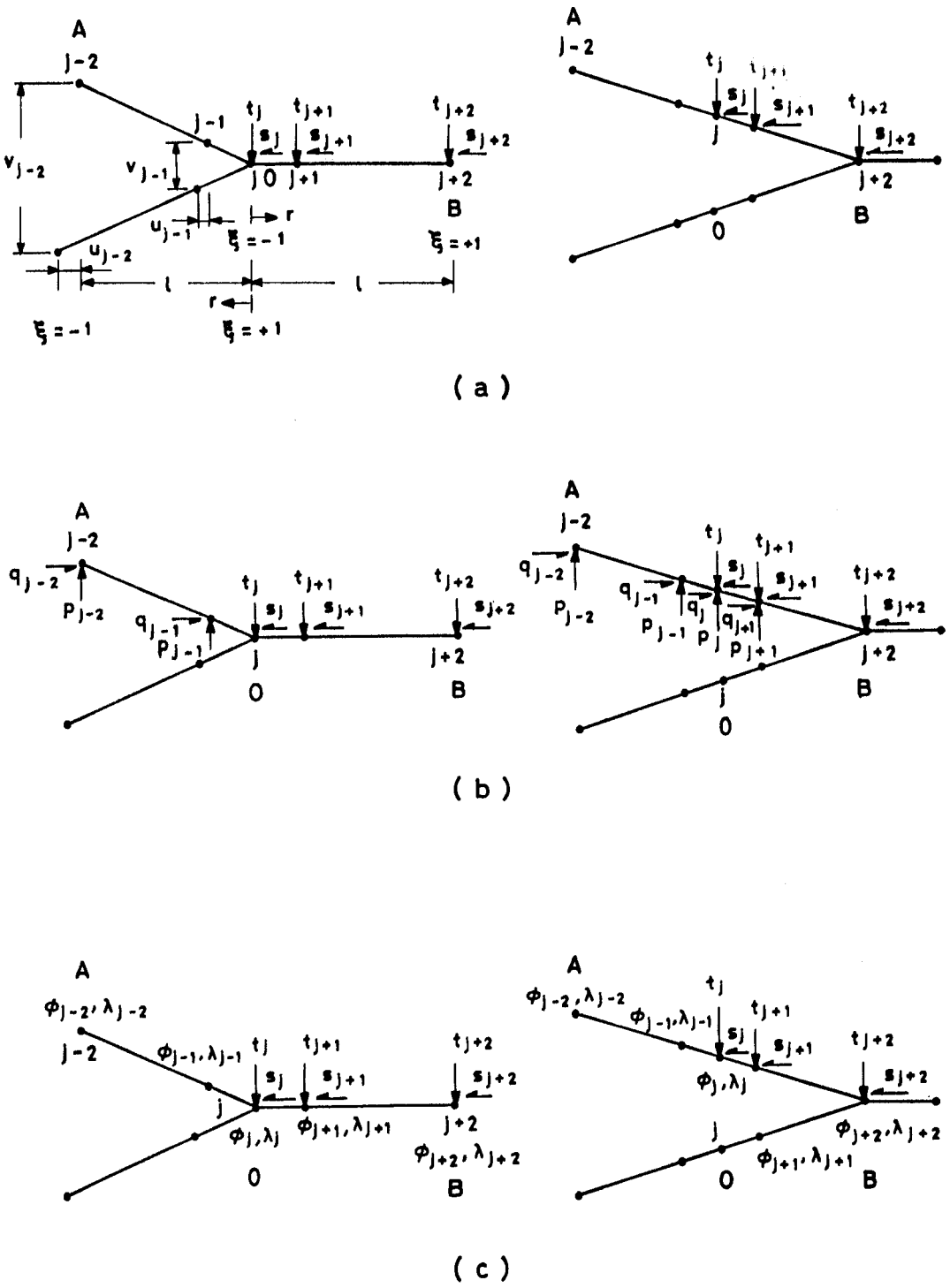

Fig. 1. Illustration of crack closure forces. (a) Remote loading, (b) crack edge loading, and (c) thermal loading.

where l is the crack tip element size, v is the crack opening and t is the traction on the ligament (OB) before the crack extension. Using Eqs. (2) and (4) the mode I strain energy release rate G_I can be evaluated.

$$G_I = [v_{j-1}\ (c_1 t_j + c_2 t_{j+1} + c_3\ t_{j+2}) + v_{j-2}(c_4\ t_j + c_5\ t_{j+1} + c_6\ t_{j+2})]/120, \tag{6}$$

where $c_1 = (180\pi - 568)$, $c_2 = (416 - 120\pi)$, $c_3 = (60\pi - 168)$, $c_4 = (164 - 45\pi)$, $c_5 = (30\pi - 48)$, and $c_6 = (44 - 15\pi)$.

Similarly the mode II crack closure work is

$$W_{II} = \tfrac{1}{2}\int_0^l us\ \mathrm{d}x, \tag{7}$$

where u is the crack sliding displacement and s is the traction in mode II direction. The mode II strain energy release rate

$$G_{II} = [u_{j-1}(c_1 s_j + c_2 s_{j+1} + c_3 s_{j+2}) + u_{j-2}(c_4 s_j + c_5 s_{j+1} + c_6 s_{j+2})]/120. \tag{8}$$

2.2. Crack edge mechanical loading

The effect of crack edge loading on the calculation of crack closure work is discussed by Mukhopadhyay et al. [23]. As the crack extends up to B (Fig. 1b), the newly formed crack edges become also subjected to the same crack edge loading. An additional amount of work is to be done to close the extended crack. For an uniform fluid pressure on the crack edge, for example, the mode I crack closure work

$$W_I = \tfrac{1}{2}\int_0^l vt\ \mathrm{d}x + \tfrac{1}{2}\int_0^l vp\ \mathrm{d}x, \tag{9}$$

where p is component of fluid pressure in mode I direction. The mode I and mode II energy release rates for this case are

$$G_I = [v_{j-1}\ (c_1\ t_j + c_2\ t_{j+1} + c_3\ t_{j+2} + c_4\ p) + v_{j-2}\ (c_5\ t_j + c_6\ t_{j+1} + c_7\ t_{j+2} + c_8\ p)]/120, \tag{10}$$

$$G_{II} = [u_{j-1}\ (c_1\ s_j + c_2\ s_{j+1} + c_3\ s_{j+2} + c_4\ q) + u_{j-2}\ (c_5\ s_j + c_6\ s_{j+1} + c_7\ s_{j+2} + c_8\ q)]/120, \tag{11}$$

where $c_1 = (180\pi - 568)$, $c_2 = (416 - 120\pi)$, $c_3 = (60\pi - 168)$, $c_4 = 40$, $c_5 = (164 - 45\pi)$, $c_6 = (30\pi - 48)$, $c_7 = (44 - 15\pi)$ and $c_8 = 20$.

2.3. Thermal loading

To analyse a thermal stress problem, the temperatures and temperature gradients are required at all the boundary nodes. Further, for solving a mixed mode problem adapting the subregion technique, equal temperatures, and equal and opposite temperature gradients, are

specified along all the nodes of the common interfaces of any two adjacent subregions. Obviously, during an analysis all nodes on the crack edges, outer boundary and interfaces are subjected to thermal loads which are all known. As the crack extends to B (Fig. 1c), the newly formed crack edges are not subjected to any new thermal loading. That is, before and after the crack extension the temperatures (ϕ_j, ϕ_{j+1}, ϕ_{j+2}) and gradients (λ_j, λ_{j+1}, λ_{j+2}) are the same at the nodes j, $j+1$ and $j+2$. The procedure for computation of the SIFs based on the MCCI technique for a such loading is discussed in [24]. It is sufficient to note here that the strain energy release rates for mode I and mode II can be evaluated using Eqs. (6) and (8), where the tractions (t_j, s_j), (t_{j+1}, s_{j+1}), etc., are the usual tractions calculated through the BEM.

For a problem with thermal as well as mechanical loads on the crack edges, e.g. fluid pressure, as the crack extends, the newly formed crack edges will be subjected to the same fluid pressure. This load on the crack edge will contribute to an extra crack closure work. However, there is no additional contributions due to the thermal load arising out of the changed boundary configuration. The strain energy release rates for mode I and mode II can be computed by Eqs. (10) and (11).

3. Case studies on mechanical loading

Five case studies, involving mode I or mixed mode mechanical loading, are presented. The plane strain condition is assumed throughout. The material is assumed to be isotropic with elastic modulus $E = 210$ GPa and Poisson's ratio $\mu = 0.3$. All computations have been performed using eight-point Gaussian quadrature.

3.1. Centre and edge cracks under mode I

For the centre crack problem (Fig. 2a) the a/W ratio is studied in the range 0.2–0.8. One fourth of the plate is modelled using 22 quadratic elements. The crack tip element size is considered as $0.01a$. The computed SIF correction factor Y ($Y = K_I/\sigma\sqrt{\pi a}$) for the entire range of a/W is tabulated in Table 1. The results are compared with the reference solutions [25] which are accurate within 1%. The proposed MCCI scheme gives a maximum error of 2.3% for the entire range 0.2–0.8 of a/W. This problem was earlier studied [22] employing only the strain singularity element where the maximum error was reported to be 3.8%. The importance of both the strain and traction singularities is therefore evident.

For the edge crack (Fig. 2b) $\theta = 0^\circ$ and $H_1 = H_2$. The range of a/W considered is 0.2–0.7. The earlier discretisations are again employed. The computed SIF correction factor Y ($Y = K_I/\sigma\sqrt{\pi a}$) are compared with the reference solutions [25] in Table 1. The maximum error for the entire range of a/W is 1%. It may be noted here that the maximum error is 2.2% when only the strain singularity is modelled [22].

3.2. Angled crack

The major dimensions are $H_1 = H_2 = 20$ mm (Fig. 2b) and $a/W = 0.5$. The crack angle is

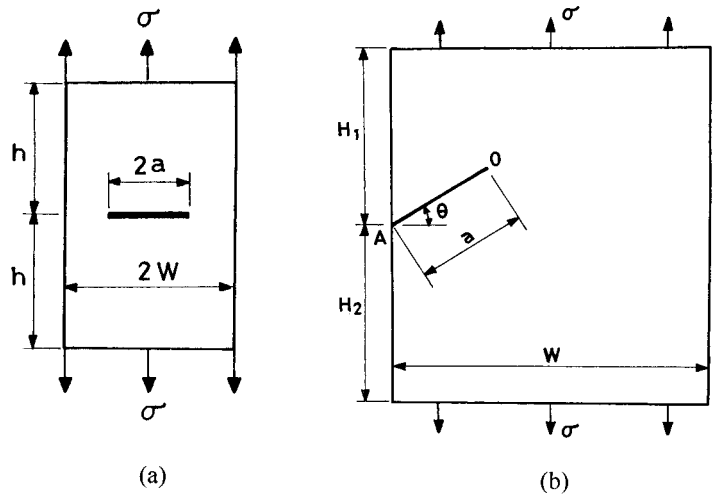

Fig. 2. (a) Centre crack, and (b) edge crack under mechanical loading.

varied from 15 to 60°. The domain is divided into two subregions. Each subregion is modelled using 25 elements. The crack tip element size is $0.02a$. The detail of mesh is available elsewhere [23]. The computed SIF correction factor Y ($Y = K_I/\sigma\sqrt{\pi a}$ or $Y = K_{II}/\sigma\sqrt{\pi a}$) are compared (Table 2) with the solutions presented in Rooke and Cartwright [26] and Sethuraman [27]. The agreement is good.

3.3. Tee joint with edge crack

The tee joint is examined when it is subjected to a bending moment (Fig. 3). The a/W ratio is considered in the range 0.1–0.5. The subregion technique is used again. The domain is divided into two subregions. The boundary element mesh is shown in Fig. 7. The crack tip

Table 1
Comparison of SIF correction factor Y for centre crack and edge cracks under mode I

a/W	SIF correction factor Y					
	Centre crack			Edge crack		
	Murakami [25]	Y	Error (%)	Murakami [25]	Y	Error (%)
0.2	1.0254	1.0098	−1.520	1.3736	1.3643	−0.674
0.3	1.0594	1.0431	−1.542	1.6629	1.6581	−0.286
0.4	1.1118	1.0958	−1.438	2.1066	2.1095	0.139
0.5	1.1891	1.1713	−1.498	2.8297	2.8194	−0.365
0.6	1.3043	1.2804	−1.833	4.0299	4.0184	−0.286
0.7	1.4842	1.4523	−2.149	6.3610	6.2912	−1.098
0.8	1.7989	1.7577	−2.288			

Table 2
Comparison of SIF correction factor Y for angled crack

θ	Mode	SIF correction factor Y			
		Rooke et al. [26]	Sethuraman [27]	Y	Error (%)
15.0	I		2.5476	2.5601	
15.0	II		0.3696	0.3623	
22.5	I	2.2800	2.2547	2.2741	−0.258
22.5	II	0.4950	0.5003	0.4880	−1.423
30.0	I		1.9056	1.9361	
30.0	II		0.5788	0.5614	
45.0	I	1.2000	1.2305	1.2524	4.370
45.0	II	0.5700	0.5850	0.5675	−0.437
60.0	I			0.6797	
60.0	II			0.4494	

element size is $0.02a$. Watson [15] analysed a similar tee joint assuming a curved crack. Mukhopadhyay et al. [24] have also analysed the similar problem assuming the crack to be a straight one and using the strain singularity element. The SIF correction factors Y ($Y = K_I/\sigma\sqrt{\pi a}$ or $Y = K_{II}/\sigma\sqrt{\pi a}$) are presented in Table 3. In this case, σ is taken as 1 MPa. The results show that the mode I SIF is significant. The mode I SIFs lie in between the results of Watson [15] and Mukhopadhyay et al. [24].

3.4. Gear tooth with edge crack

A gear with module $m = 5$ and number of teeth = 12 (i.e. pitch circle diameter 60 mm) is studied (Fig. 4a). The face width of the gear is 1 mm. A crack is considered at an angle 45°. The ratio a/W ($W = 12.217872$ mm) is studied in the range 0.1–0.5. The gear tooth is divided

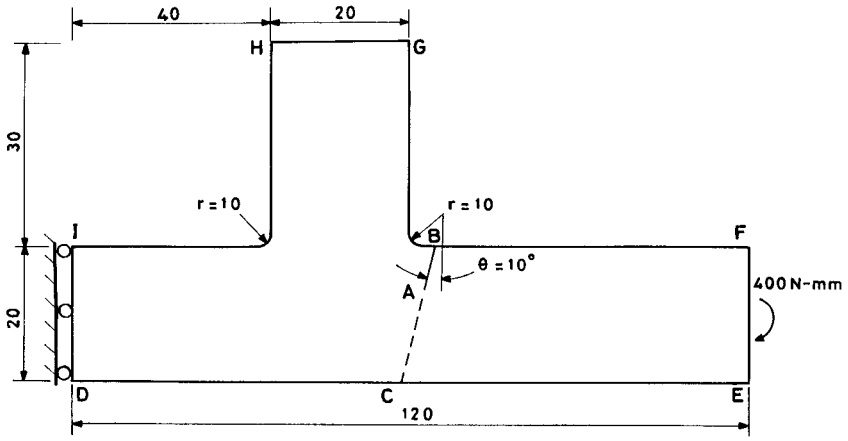

Fig. 3. Tee joint with edge crack under mechanical loading.

Table 3
Comparison of SIF correction factor Y for tee joint with edge crack

a/W	Mode	SIF correction factor Y		
		Watson [15]	Mukhopadhyay et al. [24]	Present
0.1	I	6.8630	7.0712	6.9684
0.1	II		0.0144	0.0144
0.2	I	6.4160	6.6079	6.5188
0.2	II		0.1798	0.1779
0.3	I	6.6160	6.7949	6.7072
0.3	II		0.3129	0.3091
0.4	I	7.2770	7.4792	7.3874
0.4	II		0.4341	0.4289
0.5	I	8.5140	8.7656	8.6666
0.5	II		0.5685	0.5620

into two subregions ABCDEFGHIJKLA and MNODCBM (Fig. 4b). The regions ABCDEFGHIJKLA and MNODCBM are modelled using 37 and 28 elements, respectively. The gear tooth profiles EF and GH are approximated as shown in Fig. 4a. EF and FG are modelled using three quadratic elements. The tooth profile is joined with base using a fillet of $r = 1.5$ mm. The fillets JK and EDO are modelled using two and four elements, respectively, of equal angles. The crack edge is divided into six elements. The crack tip element size is $0.02a$. The subsequent elements away from the crack tip are 0.04, 0.08, $0.16a$, etc. Seven elements are employed to discretise the remaining ligament for all the a/W ratios. All nodes on the edges AL and MN are fixed in both x- and y-directions. A load of 100 N/mm is applied normally at the top element of the tooth profile FG (Fig. 4b). The computed SIF correction factor Y ($Y = K_{\mathrm{I}}/\sigma_{\mathrm{b}}\sqrt{\pi a}$ or $Y = K_{\mathrm{II}}/\sigma_{\mathrm{b}}\sqrt{\pi a}$) are presented in Table 4. σ_{b} is the Lewis bending stress [28]

Table 4
SIF correction factor Y for gear with edge crack

a/W	Mode	Y for various types of elements			
		Linear	Quadratic	Strain singularity	Traction singularity
0.1	I	0.5035	0.5306	0.5148	0.5229
0.1	II	0.0666	0.0693	0.0674	0.0684
0.2	I	0.3851	0.4050	0.3932	0.3992
0.2	II	0.0958	0.1001	0.0973	0.0988
0.3	I	0.3215	0.3380	0.3282	0.3332
0.3	II	0.1153	0.1207	0.1173	0.1191
0.4	I	0.2707	0.2848	0.2766	0.2807
0.4	II	0.1288	0.1351	0.1313	0.1334
0.5	I	0.2203	0.2320	0.2252	0.2285
0.5	II	0.1370	0.1440	0.1400	0.1421

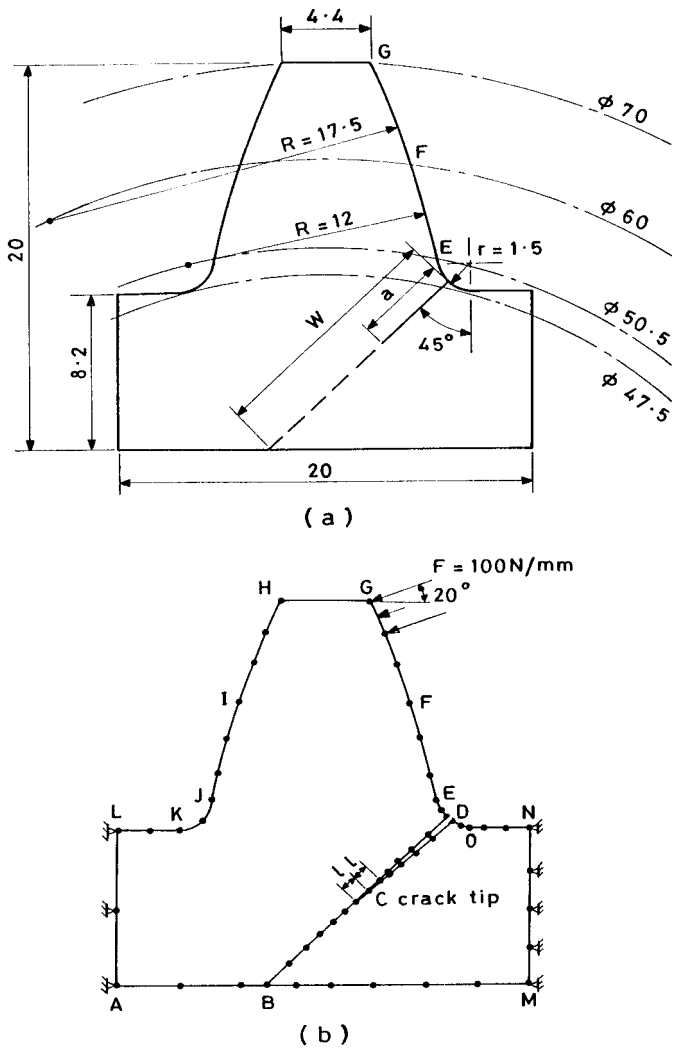

Fig. 4. Gear tooth with edge crack. (a) Geometry, and (b) boundary element mesh.

and is equal to $F\cos\vartheta\pi/(tpY_l)$, where F is the total load, p is circular pitch, Y_l is the Lewis form factor and ϑ is gear tooth pressure angle. In this case Y_l is 0.245 [28] and σ_b is calculated as 136.77 N/mm^2.

No reference solution is available for a comparison. The SIF correction factor is compared with the values obtained by employing separately the linear, quadratic and strain singularity elements (Table 4). The mode I loading is more dominant than the mode II. The mode I SIF correction factor Y decreases with an increase in the a/W ratio while the mode II Y increases. The results based on the modelling of both the strain and traction singularities show a maximum difference of 1.6% with those due to modelling of only the strain singularity.

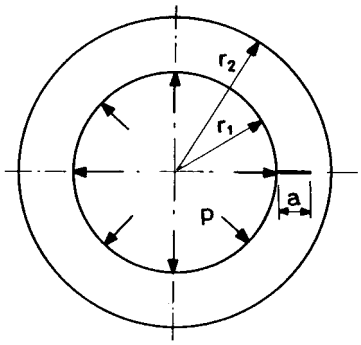

Fig. 5. Cylinder with radial inner edge crack under internal pressure.

3.5. Cylinder with radial crack under internal pressure

Parameter $a/(r_2-r_1)$ is considered in the range 0.2–0.8 (Fig. 5). The sizes of the element near the crack tip are 0.01, 0.02, 0.04, 0.08a, etc. The computed SIF correction factor Y ($Y = K_I/p\sqrt{\pi a}$) are compared with the reference solutions [25] in Table 5. The computed Y indicates a maximum error 2.6% for the whole range of a/W. The same error is around 4.1% [23] when only the strain singularity is modelled.

4. Case studies on thermal loading

Three case studies of mode I, mode II and mixed mode are presented. For all the three cases temperature and heat fluxes are first computed using potential boundary element formulation. In the second stage the stress analysis is performed. As before the plane strain condition is assumed.

Emery et al. [16] have shown that the near field solution of temperature around the crack tip is given by

$$\phi(x,\ y) = K_T r^n \sin n\theta, \tag{12}$$

Table 5
Comparison of SIF correction factor Y for cylinder with radial crack under internal pressure

a/W	Murakami [25]	Present	Error (%)
0.2	2.7760	2.7274	−1.749
0.3	2.8672	2.8127	−1.899
0.4	2.9887	2.9368	−1.737
0.5	3.1360	3.0671	−2.197
0.6	3.3152	3.2455	−2.101
0.7	3.5541	3.4624	−2.582
0.8	3.9125	3.8210	−2.338

where $n = 1/2, 1, 3/2$, etc. Here $\phi(x, y)$ denotes the temperature and K_T is the amplitude of thermal singularity. Obviously, $n = 1/2$ indicates a singularity in temperature derivative $(\partial\phi/\partial r)$ and heat flux $(\partial\phi/\partial n)$ at the crack tip. The singularity in heat flux may be modelled in the same way as the traction singularity, i.e.

$$\lambda = \underline{N}_1\underline{\lambda}_1 + \underline{N}_2\underline{\lambda}_2 + \underline{N}_3\underline{\lambda}_3. \tag{13}$$

When this heat flux singularity element is employed in the potential analysis, the computed fluxes λ_j and λ_{j+1} are different from the actual derivatives. The temperature field can be represented by an equation of the type of Eq. (1).

4.1. Centre crack under mode I

For a centre crack under mode I thermal loading (Fig. 6a) a/W ratio is varied from 0.1 to 0.6. The major dimensions and properties chosen are: $L = W = 40$ mm, elastic modulus $E = 1$ MPa, Poisson's ratio $\nu = 0.3$ and coefficient of linear expansion $\alpha = 10^{-4}/^{\circ}\text{C}$. No restraint is applied on the deformation of the plate. The crack edge is maintained at a temperature $\phi_1 = 0^{\circ}\text{C}$. The outer edges of the plate is maintained at $\phi_2 = 100^{\circ}\text{C}$. One quarter of the plate ABCD is modelled using 23 elements. The crack tip element size is $0.02a$. The computed SIFs are presented in Table 6. Table 6 also includes the results due to Sumi and Katayama [29]. The temperature distribution around the crack tip is symmetric and the heat flux is zero along the remaining portion of the ligament ahead of the crack. The application of special heat flux singularity element produces no effect in this problem. This is expected because the heat flux normal to the crack line is zero. The maximum error in the SIF is around 2.6% from the solutions [29] for the entire range of $a/W = 0.1$–0.6. The reported maximum error employing only the strain singularity element is about 4.4% [24].

4.2. Centre crack under mode II

In this example (Fig. 6b) a/W ratio is varied from 0.1 to 0.6. The top and bottom edges ED

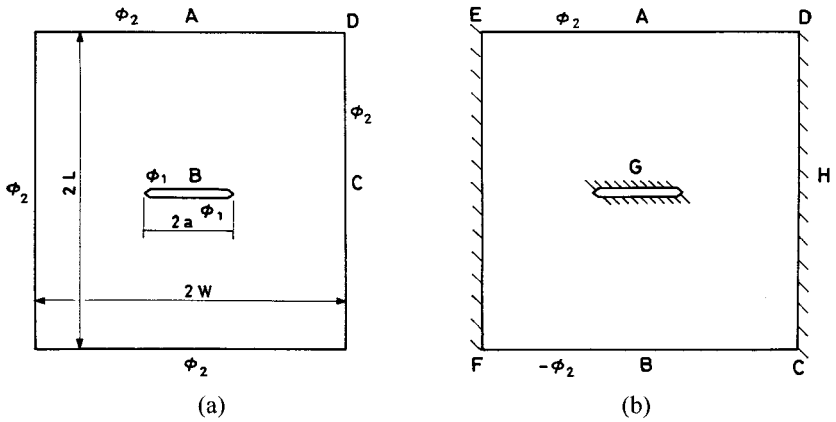

Fig. 6. Centre crack under (a) mode I, and (b) mode II thermal loading.

Table 6
Comparison of SIFs for centre crack under mode I and mode II thermal loading

a/W	Mode I centre crack			Mode II centre crack		
	Ref. [29]	SIF	Error (%)	Ref. [29]	Y	Error (%)
0.1	0.01739	0.01706	−1.916	0.0210	0.0197	−6.091
0.2	0.02213	0.02189	−1.072	0.0530	0.0527	−0.494
0.3				0.0940	0.0933	−0.790
0.4	0.02909	0.02839	−2.589	0.1410	0.1378	−2.268
0.5	0.03099	0.03101	0.049	0.1880	0.1855	−1.350
0.6	0.03320	0.03315	−0.141	0.2470	0.2380	−3.646

and FC are maintained at temperature ϕ_2 and $-\phi_2$, respectively. The edges FE and DC and the crack edges are insulated. The chosen data are $\phi_2 = 10°C$, $E = 2.184 \times 10^5$ Pa, $\nu = 0.3$, $\alpha = 1.67 \times 10^{-5}/°C$ and $L/W = 1$. One half of the plate ABCD is modelled. The subregion technique is adapted for the analysis. Each region is discretised by 20 elements. The crack tip element size is $0.04a$. The temperature distribution is anti-symmetric with respect to the crack line. There are singularities in both temperature gradient and heat flux. Employing heat flux singularity element the temperature and the heat fluxes are computed. Using these data the stress analysis is done to obtain the SIFs. The SIFs are nondimensionalised, $Y = \mathrm{SIF}/F$, where $F = \alpha\phi_2 E W^{0.5}$. The correction factor Y is compared with the reference solution [29] in Table 6. The maximum difference is around 3.6% for the range of $a/W = 0.2$–0.6. For this example the maximum error by only the strain singularity element is about 5.9% [24].

4.3. Tee joint with edge crack

The tee joint considered earlier is again analysed (Figs. 3 and 7). The case is studied under thermal and/or mechanical loading. The edges ID and EF are considered to be restrained in

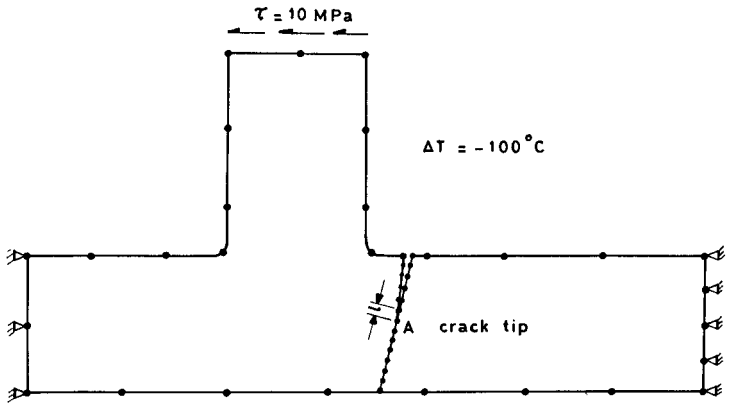

Fig. 7. Tee joint with edge crack under thermal and mechanical loading.

both the x and y directions. The material properties are: $E = 2.1 \times 10^5$ MPa, $\nu = 0.3$ and $\alpha = 1.2 \times 10^{-5}/^{\circ}$C. The temperature of the whole body is considered to drop by 100°C uniformly. On top of this thermal loading, the joint is subjected to a uniform shear load $\tau = 10$ MPa on the edge GH. The computed SIF correction factors Y ($Y = K_I/\sigma\sqrt{\pi a}$ or $Y = K_{II}/\sigma\sqrt{\pi a}$, where σ is taken as 1 MPa) considering only the thermal load and both thermal and mechanical load are presented in Table 7. The results are compared with the solutions presented in [24]. With only the thermal load, the mode I correction factor Y initially decreases up to $a/W = 0.2$ and then increases. The mode II correction factor Y steadily increases. The mode I SIF is dominant. Similar trend is observed when both mechanical and thermal loads are considered.

5. Effect of crack tip element size on accuracy

The effect of crack tip element size on the accuracy of SIF computation using the traction singularity element is studied considering the examples of centre crack under mechanical load, edge crack under mechanical load and mode I centre crack under thermal load. The a/W ratios selected are 0.5, 0.5 and 0.2, respectively. For all the three cases the crack tip element size l is varied from 0.02 to 0.2a. The errors in the computed SIFs are shown in Fig. 8. The straight lines refer to the best fits. The results show that for mechanical loading, the accuracy of the proposed formulation is not very much dependent on l/a. For example, for the centre crack under mechanical load the error is almost constant. The variation is approximately from −1.5 to −1.75% for the entire range of l/a. A similar trend is again observed for the edge crack under mechanical load. Here the error varies from −0.4 to −0.6% for the whole range of l/a. In case of thermal loading, the dependency is more. In the mode I centre crack under thermal loading the error varies from −1.5% at $l/a = 0.02$ to −4.5% at $l/a = 0.2$. The error is around

Table 7
SIF correction factor Y for tee under thermal and/or mechanical loads

a/W	Mode	SIF correction factor Y			
		Thermal load		Thermal and mechanical loads	
		Ref. [24]	Present	Ref. [24]	Present
0.1	I	508.06	500.72	561.03	552.92
0.1	II	16.86	16.64	12.99	12.83
0.2	I	498.04	491.33	544.08	536.74
0.2	II	35.63	35.19	30.89	30.51
0.3	I	515.34	508.51	556.70	549.30
0.3	II	46.11	45.51	40.99	40.45
0.4	I	534.25	527.11	571.02	563.36
0.4	II	50.97	50.27	45.52	44.89
0.5	I	539.55	532.21	570.83	563.00
0.5	II	51.43	50.68	45.47	44.80

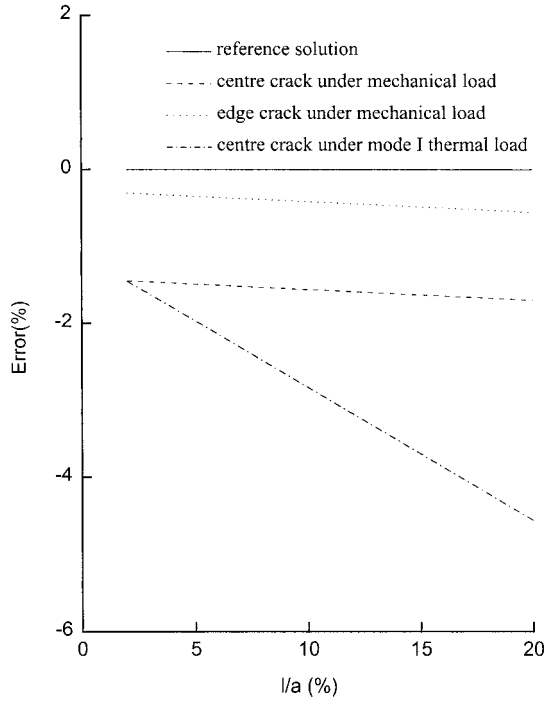

Fig. 8. Effect of crack tip element size on accuracy for traction singularity element.

-2.8% for $l/a = 0.1$. In the case of thermal loading, there is a little more dependency. The MCCI based calculation of SIF in general offers flexibility in the choice of size of the crack tip element. A crack tip element size of 8–10% of crack size is recommended. It must be emphasised that the displacement method will not offer this flexibility.

6. Effect of order of Gaussian quadrature

When both the heat flux and temperature derivative singularities are modelled at the crack tip, the fundamental solution is multiplied by $\sqrt{(l/r)}$ making the order of singularity $[\ln(1/r) \times \sqrt{(1/r)}]$. For the elastic analysis employing the traction singularity element, the order of singularity is again $[\ln(1/r) \times \sqrt{(1/r)}]$. In the thermoelastic stress analysis the order of singularity in the traction and strain is $[\ln(1/r) \times \sqrt{(1/r)}]$ and $[\ln(r) \times \sqrt{(1/r)}]$ respectively. The order of quadrature has a significant influence on the results. This is presented in Tables 8 and 9 when the number of Gauss points are varied from 4 to 16 [30]. For the mode I centre crack under mechanical load (Table 8) the effect on the accuracy of results is insignificant. A similar trend is observed for the case of cylinder with radial crack (Table 8).

In the mode I centre crack under thermal load the effect of order of quadrature on the accuracy is pronounced (Table 9). The maximum error is around 5.3% when number of Gauss points $N = 4$. This reduces to around 2.6% when order is increased to 16. In the mode II

Table 8
Effect of order of Gauss integration scheme on accuracy of SIFs for mechanical loading

a/W	Difference in SIF (%) (order of Gaussian quadrature)			
	$N = 4$	$N = 8$	$N = 12$	$N = 16$
Mode I edge crack				
0.2	−0.688	−0.674	−0.674	−0.673
0.3	−0.294	−0.286	−0.285	−0.285
0.4	0.132	0.139	0.140	0.141
0.5	−0.367	−0.365	−0.364	−0.363
0.6	−0.320	−0.286	−0.284	−0.284
0.7	−1.187	−1.098	−1.096	−1.096
Cylinder with radial crack				
0.2	−1.476	−1.749	−1.758	−1.758
0.3	−1.877	−1.899	−1.899	−1.899
0.4	−1.761	−1.737	−1.736	−1.736
0.5	−2.234	−2.197	−2.195	−2.195
0.6	−2.080	−2.101	−2.099	−2.099
0.7	−2.420	−2.582	−2.575	−2.575
0.8	−1.920	−2.338	−2.367	−2.363

centre crack under similar trend is evident. Here also the accuracy improves as the order is increased. For $a/W = 0.1$, the difference improves from 13.8% for $N = 4$ to 6% for $N = 16$. In general a reasonable accuracy can be attained by using an order of integration equal to 8.

Table 9
Effect of order of Gauss integration scheme on accuracy of SIFs for thermal loading

a/W	Difference in SIF (%) (order of Gaussian quadrature)			
	$N = 4$	$N = 8$	$N = 12$	$N = 16$
Mode I centre crack				
0.2	−5.261	−2.776	−2.196	−1.916
0.3	−3.069	−1.721	−1.285	−1.072
0.4	−4.050	−3.064	−2.745	−2.589
0.5	−1.268	−0.378	−0.091	0.049
0.6	−1.339	−0.519	−0.265	−0.141
Mode II centre crack				
0.1	−13.826	−9.130	−7.092	−6.091
0.2	−6.389	−2.414	−1.129	−0.494
0.3	−4.876	−2.128	−1.234	−0.790
0.4	−5.339	−3.271	−2.599	−2.268
0.5	−3.810	−2.154	−1.615	−1.350
0.6	−5.600	−4.286	−3.858	−3.646

7. Conclusions

The effect of modelling of singularities in the derivative of field variable and the flux or traction simultaneously has been brought out through a number of case studies. Mode I, mode II and mixed mode examples under remote mechanical loading, crack edge loading and thermal loading are considered to demonstrate the effect. The accuracy of the computed SIFs improves over the results obtained by only the strain singularity elements. The effect of partial/full modelling is more pronounced in the case of thermal loading than in the case of pure mechanical loading. The MCCI based computation of SIF offers flexibility in the selection of size of the crack tip element. A crack tip element size up to 8–10% of crack size can be employed to obtain results with a reasonably good accuracy. While modelling both traction and strain singularities a moderate order of Gaussian quadrature (about 8) is recommended.

References

[1] Barsoum RS. On the use of isoparametric finite elements in linear fracture mechanics. Int J Numer Meth Eng 1976;10:25–37.
[2] Cruse TA, Wilson RB. Advanced applications of boundary-integral equation methods. Nucl Eng Des 1978;46:223–34.
[3] Tan CL, Fenner RT. Elastic fracture mechanics analysis by the boundary integral equation method. Proc R Soc London A 1979;369:243–60.
[4] Xanthis LS, Bernal MJM, Atkinson C. The treatment of singularities in the calculation of stress intensity factors using the boundary integral equation method. Comput Meth Appl Mech Eng 1981;26:285–304.
[5] Blandford GE, Ingraffea AR, Ligget JA. Two dimensional stress intensity factor computations using the boundary element method. Int J Numer Meth Eng 1981;17:387–404.
[6] Nadiri F, Tan CL, Fenner RT. Three-dimensional analyses of surface cracks urised thick walled cylinders. Int J Pres Ves Piping 1982;10:159–67.
[7] van der Weeen F. Mixed mode fracture analysis of rectilinear anisotropic plates using singular boundary elements. Comput Struct 1983;17:469–74.
[8] Martinez J, Dominguez J. On the use of quarter-point boundary elements for stress intensity factor computations. Int J Numer Meth Eng 1984;20:1941–50.
[9] Aliabadi MH, Rooke DP, Cartwright DJ. An improved boundary element formulation for calculating stress intensity factors: application to aerospace structures. J Strain Anal 1987;22:203–7.
[10] Gangming L, Yongyuan Z. Application of boundary element method with singular and isoparametric elements in three dimensional crack problems. Eng Fract Mech 1988;29:97–106.
[11] Gangming L, Yongyuan Z. Improvement of stress singular element for crack problems in three dimensional boundary element method. Eng Fract Mech 1988;31:993–9.
[12] Aliabadi MH, Rooke DP, Cartwright DJ. Fracture-mechanics weight-functions by the removal of singular fields using boundary element analysis. Int J Fract 1989;40:271–84.
[13] Zang WL, Gudmundson P. Contact problems of kinked cracks modelled by a boundary integral method. Int J Numer Meth Eng 1990;29:847–60.
[14] Saez A, Gallego R, Domingeuz J. Hypersingular quarter-point boundary elements for crack problems. Int J Numer Meth Eng 1995;38:1681–701.
[15] Watson JO. Singular boundary elements for the analysis of cracks in plane strain. Int J Numer Meth Eng 1995;38:2389–411.
[16] Emery AF, Neighbors PK, Kobayashi AS, Love WJ. Stress intensity factors in edge-cracked plates subjected to transient thermal singularities. J Pres Ves Tech 1977;99:100–5.

[17] Chao CK, Chang RC. Crack trajectories influenced by mechanical and thermal disturbance in anisotropic material. Theor Appl Fract Mech 1992;17:177–87.
[18] Katsareas DE, Anifantis K. On the computation of mode I and II thermal shock stress intensity factors using a boundary-only element method. Int J Numer Meth Eng 1995;38:4157–69.
[19] Prasad NNV, Aliabadi MH, Rooke DP. Effect of thermal singularities on stress intensity factors: edge crack in rectangular and circular plate. Theor Appl Fract Mech 1996;24:203–15.
[20] Farris TN, Liu M. Boundary element crack closure calculation of three-dimensional stress intensity factors. Int J Fract 1993;60:33–47.
[21] Maiti SK, Mukhopadhyay NK, Kakodkar A. Boundary element method based computation of stress intensity factors by modified crack closure integral. Comput Mech 1997;19:203–10.
[22] Mukhopadhyay NK, Maiti SK, Kakodkar A. Further considerations in modified crack closure integral based computation of stress intensity factor in BEM. Eng Fract Mech 1998;59:269–79.
[23] Mukhopadhyay NK, Maiti SK, Kakodkar A. BEM based evaluation of SIFs using modified crack closure integral technique under remote and/or crack edge loading. Eng Fract Mech 1998;61:655–71.
[24] Mukhopadhyay NK, Maiti SK, Kakodkar A. Modified crack closure integral based computation of SIFs for thermoelastic problems through BEM. Nucl. Eng. Des. 1999;187:277–90.
[25] Murakami Y, et al., editors. Stress intensity factor handbook. Pergamon Press, 1987.
[26] Rooke DP, Cartwright DJ. Compendium of stress intensity factors. London: HMSO, 1976.
[27] Sethuraman R. Analytical and finite element studies on two dimensional panels with doubly bonded rectangular finite crack stiffeners. Ph.D. thesis. Department of Mechanical Engineering, I.I.T., Bombay, India, 1989.
[28] Shigley JE. Mechanical engineering design, 2. New York: McGraw-Hill, 1963.
[29] Sumi N, Katayama T. Thermal stress singularities at tips of a Griffith crack in a finite rectangular plate. Nucl Eng Des 1980;60:389–94.
[30] Stroud AH, Secrest D. Gaussian quadrature formulas. New York: Prentice-Hall, 1966.